

Configurational Entropy Reallocation and Complex Loop Dynamics of the Mosquito-Stage Pvs25 Protein Complexed with the Fab Fragment of the Malaria Transmission Blocking Antibody 2A8

Athanasios Stavrakoudis*,† and Ioannis G. Tsoulos‡

Department of Economics, University of Ioannina, Ioannina, Greece, and Department of Communications, Informatics & Management, Technical Educational Institute of Epirus, Arta, Greece

Received September 22, 2010

Abstract: Pvs25 is a protein of unique 3D structure, and it is characterized by the presence of repeated EGF-like domains and 11 disulfide bonds. It is a very important candidate for the transmission-blocking malaria vaccine, as it plays an important role in mosquito infection by Plasmodium parasites. Recently, the X-ray structure of the protein complexed with the transmission blocking antibody 2A8 has been reported. In this study, we report the loop reorganization of the Pvs25 protein based on configurational entropy calculations and dihedral principal component analysis as revealed from the protein complex and free molecular dynamics simulations. While the total entropy of the protein was estimated to be almost the same in the free and complex trajectories, the partition of the entropy contribution in the loop fragments of the protein revealed interesting entropy reallocation after the 2A8 antibody binding. Interestingly, the 51–71 protein loop experienced a significant reduction in its configurational entropy, while other parts of the protein did not show any difference in it, or even showed an entropy increase. This trend in entropy redistribution was found to be in direct relationship with specific interactions with the antibody's binding site. Results from root-mean-square fluctuations/deviations and dihedral angle principal component analysis further support this finding.

1. Introduction

Pvs25 is a protein derived from the malaria parasite Plasmodium,^{1,2} a worldwide spread parasite.^{3,4} The protein plays an essential role in infecting mosquitoes and thus transmitting malaria.⁵ It is an important target in the development of a vaccine.^{6,7} The 3D structure of the Pvs25 protein has been solved⁸ by X-ray and is characterized by the presence of 11 disulfide bonds (Figure 1). This high number of disulfide bonds makes Pvs25 a protein of unique structure. For example, a recent review about the classification of disulfide bonds in proteins

analyzed the existence of up to 10 disulfide bonds in proteins.⁹ Given the high degree of interest in blocking the malaria transmission by mosquitoes, it is interesting to explore the dynamics of protein/antibody binding.

Computer simulation of molecular dynamics is a well established method for studying several aspects of biomolecular structure and function.^{10–12} Moreover, biomolecular modeling can complement experimental studies,¹³ and recent studies have been used in order to elucidate the dynamics of protein folding,¹⁴ to explore the immunogenicity of peptide–vaccine candidates,¹⁵ to facilitate vaccine design¹⁶ to help in rational drug design,¹⁷ to account for the peptide's flexibility in immunological complexes,¹⁸ or to dock molecules into binding sites of proteins.¹⁹ It has also been argued

* To whom correspondence should be addressed. E-mail: astavrak@cc.uoi.gr.

† University of Ioannina.

‡ Technical Educational Institute of Epirus.

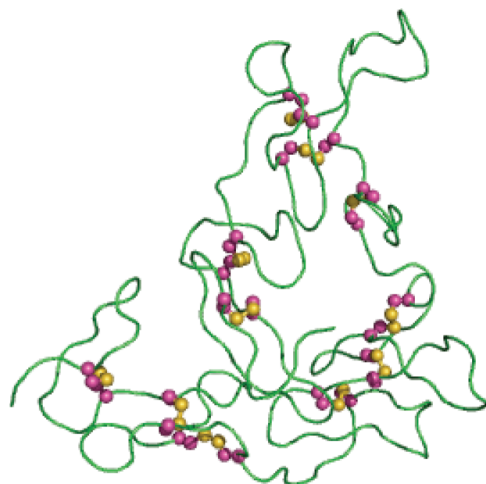


Figure 1. Ribbon representation of the X-ray structure of the Pvs25 protein. Disulfide bonds are highlighted with balls and sticks. C^α and C^β atoms of Cys residues are colored in magenta, while S^γ atoms are colored in yellow.

that molecular dynamics simulations can be used as an aiding tool in experimental studies.¹³

Biomolecular plasticity affects in an essential way many biological functions.^{20,21} The advancements in computer power and statistical mechanics methods have contributed a lot to targeting biomolecular flexibility.²² In this study, computer simulation molecular dynamics have been performed on the Pvs25 protein, and its complex with the Fab fragment of the 2A8 Fab antibody, in order to get insight into the binding mode. We have found that not all 11 disulfide loops of the Pvs25 protein behave in the same way. Differences in loop dynamics are directly related with protein/antibody contacts. The dynamics of the fourth loop, formed by Cys residues 51 and 71, are most profoundly affected. This makes the 51–71 region a candidate for engineered protein/antibody interactions in targeting the blocking of malaria transmission by mosquitoes.

2. Methods

2.1. Setup of the System and MD Simulations. Initial coordinates of the Pvs25 and the Fab fragment of malaria transmission blocking antibody 2A8 were downloaded from the Protein Data Bank,²³ PDB code: 1z3g.⁸ The protonation status of histidine side chains was estimated with the REDUCE program.²⁴ Topology and force field parameters for all atoms were assigned from the CHARMM22-CMAP parameter set.^{25,26} It has been found that the addition of cross terms with the CMAP potential improves system parametrization and helps to avoid undesired helical transitions.^{27,28} Hydrogen atoms were added with the VMD program²⁹ and its autopsf utility. The antibody/protein complex was centered in a rectangular box with dimensions $141.72 \times 87.89 \times 109.70 \text{ \AA}^3$. The box was filled with 24 429 TIP3P water molecules and neutralized with the addition of 40 Na^+ and 33 Cl^- ions to approximate a physiological ionic concentration of 0.1 mM. The total number of atoms of the whole system was 126 818. Nonbonded van der Waals interactions were gradually turned off at a distance between 12 and 14 Å. Long-range electrostatics were calculated with the PME

method.³⁰ Nonbonded forces and PME electrostatics were computed every second step. The pair list was updated every 10 steps. Bonds to hydrogen atoms were constrained with the SHAKE method,³¹ allowing a 2 fs time step for integration. The system was initially subjected to energy minimization with 5000 steps. The temperature of the system was then gradually increased to 310 K, with Langevin dynamics using the NVT ensemble, during a period of 3000 steps, by stepwise reassignment of velocities every 500 steps. The simulation was continued at 310 K for 100 000 steps (200 ps). During the minimization and equilibration phases, protein backbone atoms (N, C^α , C' , O) were restrained to their initial positions with a force constant of 50 kcal mol⁻¹ Å⁻². The system was equilibrated for another 200 ps with the force constant reduced to 50 kcal mol⁻¹ Å⁻². Finally, 400 ps of NVT simulation at 310 K were performed with total elimination of the positional restraints. The simulation was passed to the productive phase, by applying constant pressure with the Langevin piston method.³² Pressure was maintained at 1 atm and a temperature of 310 K. The results are based on a period of 20 ns of this isothermal–isobaric (NPT) run. Snapshots were saved to disk at 1 ps intervals for structural analysis. Results from this trajectory are denoted as the complex trajectory for the rest of this article.

An identical protocol was followed for the antibody-free protein (PDB code 1z27) to obtain the free trajectory of the protein.

Trajectory analysis was performed with Eucb³³ and Carma³⁴ software packages. Appropriate corrections have taken into account dealing with circular data statistics.³⁵ Hydrogen bonds were estimated with a geometrical criterion as described elsewhere.³⁶ Structural figures were prepared with PyMOL (www.pymol.org).

2.2. Dihedral Angle Principal Component Analysis. Principal component analysis (PCA) is a standard method for analyzing MD trajectories, where the reduction of the dimensionality of a high-dimensional data set is desired.³⁷ The dihedral based PCA (dPCA) has been applied^{38–40} to explore the energy landscape of a biomolecule. Calculations of dPCA have been performed with Carma.³⁴

2.3. Entropy Calculations. Molecular dynamics simulations offer various methods to estimate the absolute or relative entropy.^{41,42} Schlitter's formulation⁴³ was used for the estimation of the configurational entropy:

$$S_{\text{true}} = \frac{1}{2} k_B \ln \det \left[1 + \frac{k_B T e^2}{\hbar^2} \mathbf{M} \boldsymbol{\sigma} \right] \quad (1)$$

where S is an upper estimation of the true entropy (S_{true}), k_B is Boltzmann's constant, T is the absolute temperature (in which the system was simulated), e is the Euler number, \hbar is the Plank constant divided by 2π , \mathbf{M} is the mass matrix that holds on the diagonal the masses belonging to the atomic Cartesian degrees of freedom, and $\boldsymbol{\sigma}$ is the covariance matrix of atom positional fluctuations:

$$\sigma_{ij} = \langle x_i - \langle x \rangle \rangle \langle y_i - \langle y \rangle \rangle \quad (2)$$

Entropy calculations were performed with the backbone atoms (N, C^α , C') of the peptide from the bound and free

trajectories respectively, at 0.1 ns intervals (100 frames). Two separate trajectories (for example, free and complex trajectories of a peptide) can be combined. Thus one trajectory can be appended at the end of the other trajectory, and the plot of configurational entropy S against time can be used as an assessment of the overlap between configurational spaces sampled in the two simulations.⁴⁴ Such trajectories have been derived for the backbone (bb) atoms (N, C α , C') of the peptide from the last 10 ns of the free (f) and bound (b) trajectories. Both appending sequences were applied, resulting in S_{bb}^{trA+trB} and S_{bb}^{trB+trA} calculations, where the trB trajectory was appended to the trA one (trA+trB) or the trA trajectory was appended to the trB one (trB+trA). Plotting the calculated values of S from both the combined trajectories over time demonstrates the relative size and overlap of sampled trajectories. Plotting S over time after the combination of two trajectories results in three cases,⁴⁴ briefly described as follows:

- 1 S increases after appending one trajectory to the other, with a jump observed at this point. Thus, the two trajectories do not overlap, or there is only a small overlap between them.
- 2 S evolves smoothly after the appending of the trajectories, without an observable perturbation of the line of S over time; thus, the two trajectories show significant overlap.
- 3 The S curve increases during the time of the first trajectory but decreases a little after the appending of the second trajectory; thus, the second trajectory samples a smaller configurational space than the first one, which also contains the configurational space visited by the second one.

The calculation of entropy buildup curves has been performed with the Eucb program,³³ which utilizes a routine adapted from numerical recipes⁴⁵ for the computation of the eigenvalues. Moreover, trajectories for the backbone, heavy, or heavy side chain atoms have been extracted from the complex and free trajectories for each residue of the Pvs25 sequence, in order to obtain the entropy difference per residue.⁴⁶

2.4. Buried Surface Area. Calculation of the buried surface area (BSA) was performed with the NACCESS program,⁴⁷ based on the formula

$$\text{BSA} = S_p + S_a - S_c \quad (3)$$

Thus, the BSA is the difference of the surface accessible area of the complex (S_c) from the sum of the surface accessible areas of the protein (S_p) and antibody molecule (S_a). Calculations were performed for all frames of the complex trajectory in order to get and characterize the times series of BSA.

3. Results and Discussion

3.1. Backbone Dynamics of the Protein. The Pvs25 protein and its 2A8 antibody complex remained stable during both free and complex MD trajectories. Figure 2 shows the root-mean-square fluctuations (RMSF) of C α atoms and deviations (RMSD) of backbone (N, C α , C') atoms of the protein and antibody's heavy (H) and light chains (L).

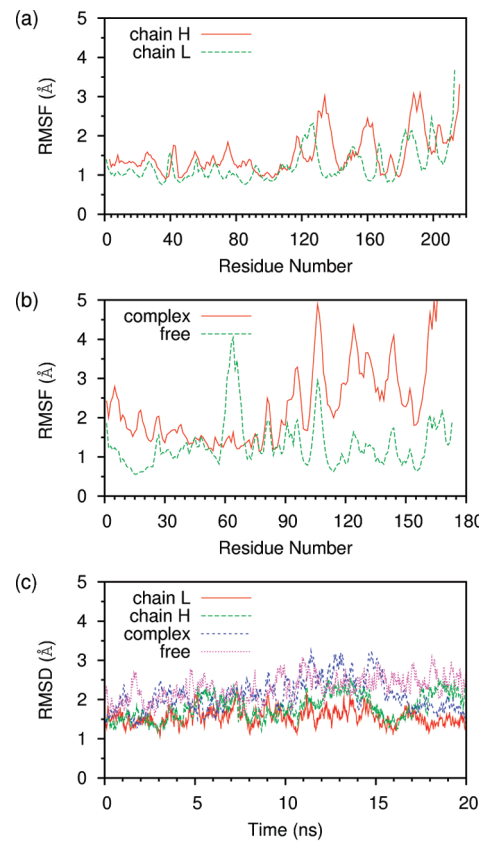


Figure 2. Root mean square fluctuation (RMSF) of C α atoms and root-mean-square deviation (RMSD) time series of backbone atoms (N, C α , C') after fitting the corresponding atom positions from MD trajectories to the initial (X-ray) coordinates. (a) RMSF of C α atoms of heavy (H) and light (L) chains of the antibody. (b) RMSF of C α atoms of the protein in complex and free forms. (c) RMSD of backbone atoms of heavy (H) and light (L) chains of the antibody, and the backbone atoms of the protein in complex and free forms.

As revealed in part c of Figure 2, the RMSD of the backbone atoms of all protein chains fluctuated between 1 and 3 Å during the simulation time, without any significant breaks or jumps. Interestingly, the Pvs25 protein showed greater mobility in comparison to antibody's heavy or light chains. The mobility of the protein's backbone atoms was found to be approximately the same in free and complex trajectories, where the average values for the RMSD (with std. dev.) were 2.3 (0.3) Å and 2.1 (0.4) Å, respectively.

An interesting feature is revealed in part b of Figure 2, where the RMSF values of the protein's C α atoms is displayed. The first 40 residues of the Pvs25 protein (N-terminal) showed more flexibility in the complex form. This picture was inversed for the next 40 residues, where comparable values were observed, or at residues around Glu₅₉ (peak of the RMSF line of protein's free trajectory), a significant reduction of the protein's C α atom's mobility was recorded. The C-terminal half of the protein showed surprisingly high mobility in the complex form. The trend of the RMSF values was very similar in the free and complex trajectories; however, the calculated values were higher in the complex than the free trajectory. In general, it is admitted that binding reduces a protein's mobility. However, in this

case, it is evident that this happened selectively in some part of the protein, while the remaining part increased its mobility.

The Pvs25 protein contains 22 Cys residues that are all paired in 11 disulfide bonds. Pvs25 is a unique protein in this respect, especially if its 177 residue length is taken into consideration. Its unique 3D structure is characterized by the presence of repeated EGF like domains.⁸ In order to see how the mobility of these disulfide loops is affected by the 2A8 binding of the Pvs25 protein, we split the protein's sequence into 11 (overlapping) parts, according to disulfide bond formation, and we measured the RMSD of the backbone atoms of these loops. The results of this procedure are displayed in Figure 3. The first three loops, 8–22, 24–36, and 42–57, did not show any difference worth mentioning in the time evolution of the RMSD. The same conclusion can be drawn for the last seven loops, 73–84, 89–100, 94–113, 115–129, 137–148, 141–157, and 159–172. The RMSD values could be very small, as in loops 8–22 and 115–129, or bigger like in loops 94–113 or 159–172, but in all of these cases, the pattern of the RMSD time evolution was very similar. This fact indicates that the antibody binding of the protein greatly influenced the intrinsic mobility of the protein's loops.

The most notable difference between the free and complex trajectories concerns the 51–71 loop. It must be underlined also that this loop contains the Glu₅₉ residue, which showed the highest RMSF value in the free trajectory (Figure 2). Thus, the 0.5 Å value that was approximately observed during the complex trajectory increased by approximately 1–1.2 Å in the free trajectory. The 51–71 disulfide loop directly contacts the antibody's heavy chain, and its reduced mobility after binding is somewhat expected. What is most notable here is that this is the only loop that is affected by the binding.

3.2. Dihedral Principal Component Analysis. In order to explore more thoroughly the backbone dynamics of the protein loops and the influence of the binding of the 2A8 antibody, we performed a principal component analysis of the complex and free trajectories, based on backbone dihedral angles. This technique has been routinely used during recent years in energy landscape studies of peptides and small proteins.^{38,39,48} At this stage, as in the RMSD calculation of the disulfide loops, we examined the energy landscape of the 11 loops of the protein, as determined by the presence of 11 disulfide bonds. The results of these calculations are illustrated in Figure 4.

Loop 8–22 showed almost identical results before and after the binding. This is also implied from the RMSD analysis, previously analyzed (Figure 3).

Loop 24–36 showed an interesting feature because of the widening of distribution in the dihedral angle space. While in the free trajectory the protein's structures clustered mainly in very close conformations, in the complex structure, a more wide distribution can be observed. The inverse picture can be seen for the 42–57 loop, where we observed a reduction in conformational space sampling upon antibody binding of the protein.

Similarly to the situation in the 34–46 loop, a significant reduction in the sampled conformational space can be

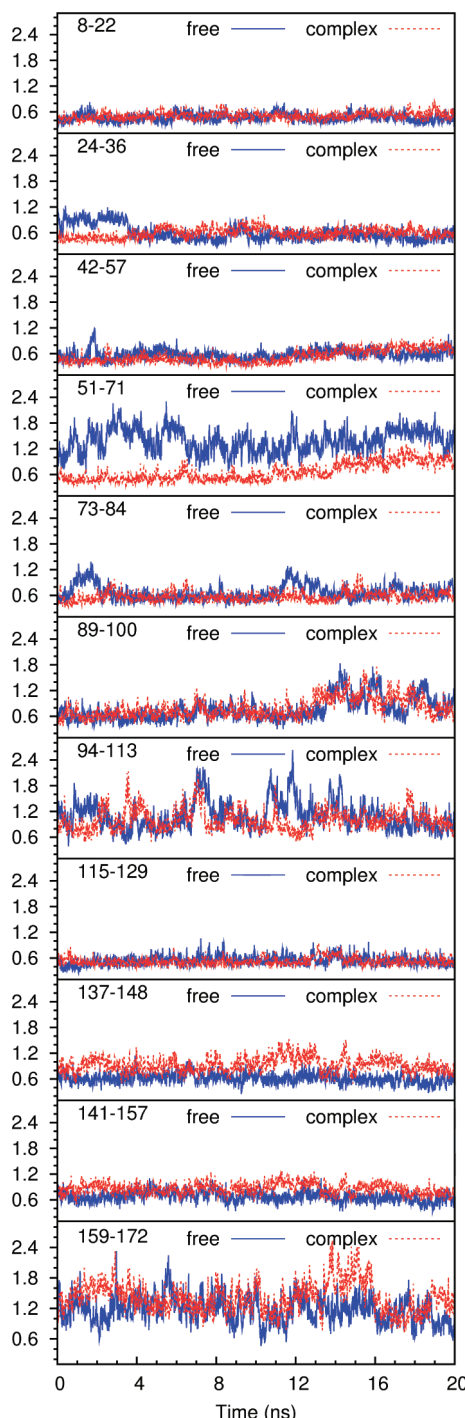


Figure 3. Time evolution of root-mean-square deviation (RMSD) of the backbone atoms of the 11 disulfide loops of the Pvs25 protein, in free and complex trajectories. RMSD is measured in Ångstroms. Numbers, e.g., 8–22, on the top left side of the plots indicate the residues that form the corresponding disulfide bond.

extracted for the 51–71 loop, from the corresponding parts of Figure 4. A second small conformational cluster is also seen in the complex trajectory. However, it seems that the antibody binding of the Pvs25 protein restricted the mobility on this fragment. The main big cluster in the complex trajectory has a center very close to those observed in the free trajectory, so it can be concluded that the 51–71 loop

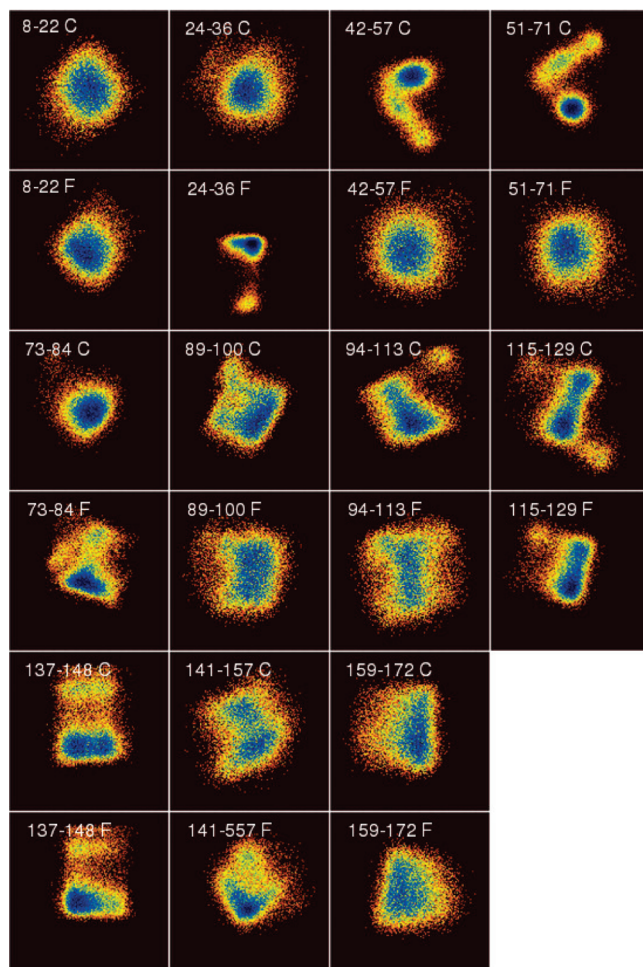


Figure 4. Dihedral principal component analysis of the 11 loops of the Pvs25 by disulfide bonds. Numbers in the plots indicate the cysteine residues that form the disulfide bonds. The letter “F” or “C” is used in order to discriminate the free or complex MD trajectory, respectively. All diagrams shown in this figure are pseudocolor representations of density functions corresponding to the projections of the fluctuations of the backbone dihedral angles (φ, Ψ) on the planes of the top two eigenvectors. The density function shown is $\Delta G = -k_B T \ln(p/p_{\max})$ where k_B is the Boltzmann constant, T is the temperature in Kelvin, and p and p_{\max} are probabilities obtained from the distribution of the principal components for each structure (frame) from the corresponding trajectory. The ΔG values obtained from this procedure are on an arbitrary scale in the sense that they depend on the binning procedure used for calculating the p and p_{\max} values. For all diagrams of this figure, the raw data were binned on a square matrix of size $N/2$, where N is the number of frames of the corresponding trajectory.

sampled, in the complex trajectory, a part of the conformational space sampled in the free trajectory.

The rest of the loops showed remarkable similarity in dihedral principal component analysis results, before and after the antibody binding.

Quite encouraging for the MD analysis process, the results from the dPCA and loop RMSD fall in line and support the hypothesis that the flexibility in the protein’s backbone, after the antibody binding, followed complex dynamics, without being uniformly distributed. Evidence is now accumulated

that the flexibility of 51–71 loop, which dominates the protein/antibody interaction interface, was considerably reduced upon antibody binding. At the same time, other parts of the protein retained almost the same flexibility, or even showed an increase of their flexibility upon binding.

3.3. Configurational Entropy Analysis. The reduction of the configurational entropy of charged residues involved in protein/protein interaction interfaces is a well-known issue.⁴⁶

We have extracted the heavy atoms of the protein from both the complex and free trajectories, and we have calculated the configurational entropies. The values we obtained were 36.31 and 36.21 $\text{kJ K}^{-1} \text{mol}^{-1}$, respectively. We also measured the configurational entropy of the backbone atoms of the protein, and we obtained values of 11.99 and 11.61 $\text{kJ K}^{-1} \text{mol}^{-1}$ for the complex and free trajectories, respectively. The negligible difference in a protein’s configurational entropy upon antibody complexation is quite interesting and deserves further investigation.

We split the protein sequence into 11 parts, as defined by the protein’s disulfide bonds, and we extracted the coordinates of the backbone atoms from both trajectories. We appended the complex trajectory to the free trajectory (and *vice versa*) for all 11 loops, and we applied a positional least-squares fitting of the combined trajectory frames’ coordinates to the first frame to remove any translational/rotational components in the configurational entropy calculations. We then calculated the configurational entropy of the combined trajectories at a 0.5 ns time interval. Then, we plotted the buildup entropy curves over time. The results of this procedure are illustrated in Figure 5. From a visual inspection of these plots, one can estimate if the conformational space sampled in the two trajectories overlapped or not, or if the two trajectories sampled different conformational spaces.

It can be easily extracted from Figure 5 that not all disulfide loops behave in the same way during the complex and free trajectories. For example, the configurational entropy of some loops located at the middle of the protein’s sequence (42–57, 51–71, 73–84, or 89–100) experienced reduced values upon complexation, while some other loops located at the C-terminal part of the protein’s sequence (137–148, 141–157, or 159–172) showed increased values upon complexation. Thus, it seems that despite the conservation of the protein’s configurational entropy upon complexation, the protein did not remain static but redistributed its flexibility in order to adapt to conformational changes imposed by the antibody binding. This observation is also in line with the RMSF calculations analyzed previously (Figure 2) and dPCA calculations (Figure 9).

The first loop, 8–22, did not show any difference in the configurational entropy upon binding. The calculated ΔS was only $-0.4 \text{ J K}^{-1} \text{mol}^{-1}$. This is in perfect agreement with the dPCA calculations of the 8–22 loop. The loops 24–36 and 42–57 showed a moderate decrease of -10.8 and $-9.8 \text{ J K}^{-1} \text{mol}^{-1}$, respectively, in the configurational entropy of the backbone atoms.

In line with the RMS (Figure 2) and dPCA (Figure 4) analysis, loop 51–71 experienced a great decrease in configurational entropy of $-54.3 \text{ J K}^{-1} \text{mol}^{-1}$. Entropy

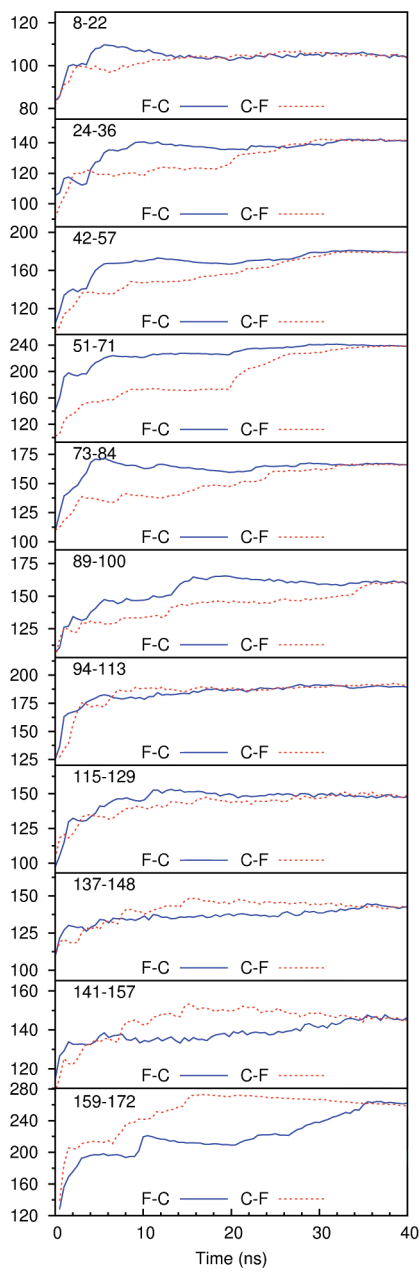


Figure 5. Configurational entropy of the 11 disulfide loops. Entropy units in the vertical axis of the plots are $J\text{ K}^{-1}\text{ mol}^{-1}$. Covariance matrices were generated after a least-squares fitting of atoms' positions of the protein to initial (X-ray) coordinates. The configurational entropy buildup curve was calculated every 500 frames (0.5 ns). The “F–C” notation indicates the appending of the complex to the free trajectory, while the “C–F” notation indicates the appending of the free to the complex trajectory.

calculations of the backbone atoms of this loop further confirmed the hypothesis that antibody binding of the Pvs25 protein greatly reduced the flexibility of this protein fragment.

Moderate entropy decreases have been observed in the 73–84 and 79–100 loops, with ΔS values of -13.1 and $-19.9\text{ J K}^{-1}\text{ mol}^{-1}$, respectively. The values are comparable with those observed for loops 24–36 and 42–57, preceding loop 51–71. As in the first loop, 8–22, the ΔS value for the 94–113 loop was found to be quite close to 0, a value of $1.1\text{ J K}^{-1}\text{ mol}^{-1}$. If we consider loop 51–71 at site 0,

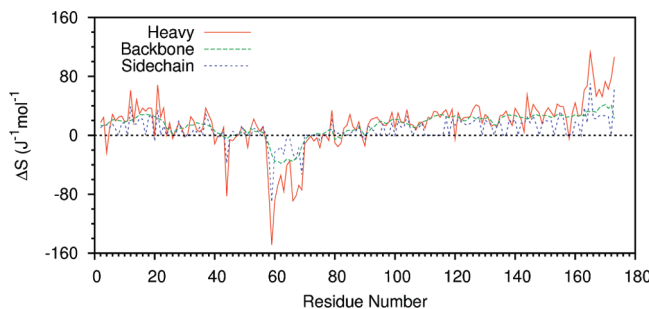


Figure 6. Differences in intraresidue configurational entropy between the complex and free trajectories measure the heavy, backbone, or side chain heavy atoms.

then loops at position $\pm 1,2$ showed a moderate decrease in ΔS and loops at position $\pm 1,2$ showed almost no difference in ΔS values upon complexation. This trend fits well with the hypothesis that the conformational flexibility restriction focused on the 51–71 loop and died out as we drew away. The trend of configurational entropy reduction fits also very well with the calculated RMSF values (Figure 2).

The remaining part of the protein showed mixed results about the ΔS . Most interesting is the increase of configurational entropies of the last two loops, 141–157 and 159–172, by 11.7 and $31.3\text{ J K}^{-1}\text{ mol}^{-1}$, respectively. The redistribution of configurational entropy^{49,50} is an important feature of the protein/antibody binding studied here.

Additional insight into the role of the configurational entropy in protein/antibody binding can be provided by examination of the per residue contribution of the configurational entropy. Figure 6 shows the intraresidue contribution in ΔS of the backbone, heavy, and heavy side chain atoms. Similarly with other analyzed observations, residues of loop 51–71 contributed with highly negative values to ΔS . Interestingly, residues of the first two loops 8–22 and 24–36 showed mostly positive ΔS values. The same conclusion can be drawn for the C-terminal part of the peptide, in line with the backbone entropy per loop difference analyzed in the preceding paragraphs. The most negative peaks of the heavy atom line correspond to residues Lys₄₄, Glu₅₉, and Val₆₆. Unsurprisingly, these residues made significant contacts with the antibody, and the reduction of their flexibility upon binding is highly expected.

The negative valley of ΔS (Figure 6) for the backbone atoms corresponds to the 58–72 sequence of the protein, which consists mostly of the 51–71 loop. There is also a small region, 43–47, of marginally negative values in the backbone entropy per residue. These findings are in excellent agreement with other parts of the MD analysis presented in this work and further corroborate the hypothesis of entropy redistribution in the binding of the Pvs25 protein by the 2A8 antibody.

The difference in the protein's configurational entropy upon antibody binding has been visualized in Figure 7. From this representation, it can be seen that region 58–69, which constituted the main region of the binding site, showed the greatest entropy reduction upon binding (colored with blue). The C-terminal end of the protein, some 45–50 Å away from the binding site, showed a considerable increase (colored red) in configurational entropy upon binding. In general, the color

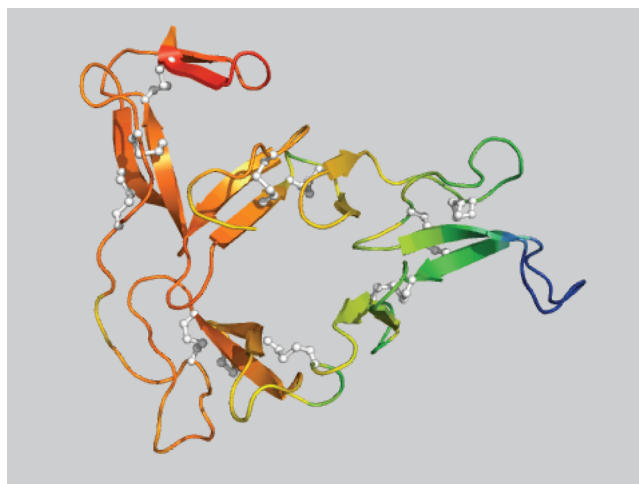


Figure 7. Ribbon representation of the X-ray structure of the Pvs25 protein. Disulfide bonds are highlighted with balls and sticks colored in white. The color spectrum in this figure represents a configurational entropy difference (complex-free) as calculated in a per residue mode (as in Figure 6) for backbone atoms. A constant value of $38.02 \text{ J kJ mol}^{-1}$ has been added to all values, to scale the entropy difference to positive values so that the B-factor column of the 1z27 PDB file could be used for the representation. Regions with blue color (like the 51–71 loop) represent negative values (entropy has been reduced upon binding), while the red color represents regions with positive values (entropy has been raised upon binding).

distribution in this figure indicates that configurational entropy redistributed smoothly in the 3D structure of the protein, from the binding site to the remote sites of the protein.

3.4. Antibody/Protein Interactions. The 2A8 antibody binds the Pvs25 protein in a discontinuous mode. Residues Lys₄₄, Leu₄₇–Gly₄₈, Gln₅₆–Cys–Ile–Glu–Asn–Pro–Asp–Pro₆₃, Gln₆₅–Val–Asn–Met–Tyr₆₉, Gly₇₂–Cys₇₃, and Glu₇₅ contact the heavy chain of the antibody. This information can be visualized with the conformational epitope database,⁵¹ URL: <http://immunet.cn/ced/view.php?cid=CE0200>.

At the center of the contact sequences lies the Glu₅₉ residue, the one with the greatest entropy change upon antibody binding of the protein. It is thus very interesting to see its interactions with the antibody. An analysis of hydrogen bonds between the protein and the antibody revealed that the side chain of the Glu₅₉ side chain formed two stable hydrogen bonds with backbone amides of the Trp_{33H} and Trp_{100H} residues from the CDR1 and CDR3 regions of the antibody's heavy chain, respectively, Figure 8. Under the light of the current analysis, it is suggested that immobilizing Glu₅₉'s side chain with two strong hydrogen bonds was the driving force behind the significant reduction in configurational entropy of the 51–71 loop.

The Lys₄₄ side chain was found in the salt bridge state with the side chain of Asp_{101H}, for 100% of the simulation time. The distance of the polar side chain atoms remained under 4.5 Å for the whole simulation time, while for 65% of the MD trajectory, a hydrogen bond between the two side chains was established. Val₆₆ made important side chain hydrophobic interactions with the antibody's Trp_{90H} and

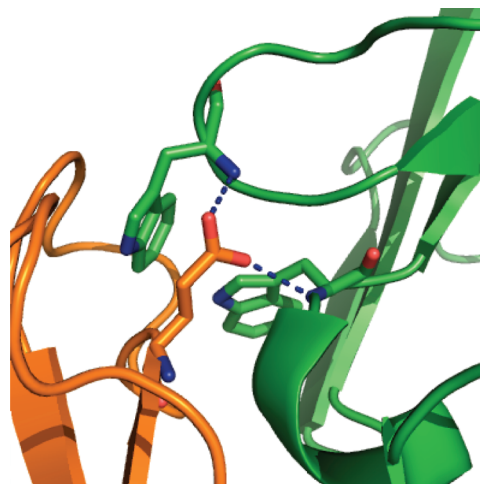


Figure 8. Interactions of the Glu₅₉ side chain of the protein with the CDR1 (Trp₃₃ on the right) and CDR3 (Trp₁₀₀ on the left) loops of the antibody's heavy chain. Hydrogen bonds of Glu's side chain carboxyl group and main chain Trp's amide group are shown with dashed lines. These hydrogen bonds remained stable through the 20 ns MD trajectory.

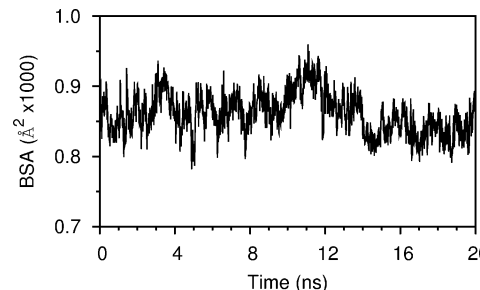


Figure 9. Time evolution of the buried surface area (BSA) between the Pvs25 protein and the 2A8 antibody, as computed from the complex directory. Calculations have been performed for all 20 000 stored frames of the MD trajectory. Data points in this plot have been averaged every 10 frames (10 ps).

Trp_{100H} side chains. The side chain distances between the Val₆₆–Trp_{90H} and Val₆₆–Trp_{90H} residue pairs were found to average at 3.7 (0.3) Å and 3.8 (0.2) Å, respectively, while the corresponding percentages of the frames with a side chain distance of less than 4 Å was 84% and 80%.

The reduction of the configurational entropy of residues making important side chain interactions has been previously noticed and analyzed with MD simulations in a protein thermostability study.⁴⁶ Here, similar observations can be drawn from the protein/antibody association.

3.5. Buried Surface Area. The buried surface area (BSA) is a useful quantity for estimating the extent and stability of protein stability of protein/protein interaction interfaces.^{52,53} Despite the concerns about the measurement accuracy of BSA,⁵⁴ it is interesting to see the value of BSA between the protein and the antibody, as evolved over the simulation time. We have calculated the BSA from the complex trajectory. The results are illustrated in Figure 9. The BSA fluctuated between 745 and 987 Å² during the MD trajectory and averaged at 861(35) Å². This average value is substantially lower than the approximately 1300 Å² observed in the X-ray

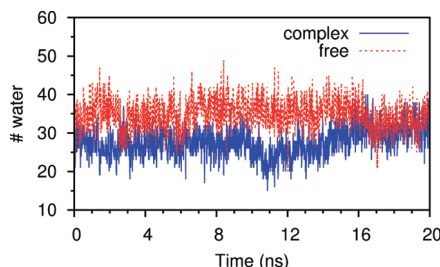


Figure 10. Time evolution of the number of water molecules within 3.3 Å of the protein's binding site. The corresponding number has been calculated for both the complex (continuous blue line) and free (dashed red line) MD trajectories. Data points in this plot have been calculated every 10 frames (10 ps).

structure of the protein/antibody complex. However, what is under investigation here is the stability of the complex, and this can be confirmed by the absence of any trend line in the time series of the BSA. For example, it has been proposed that the BSA decline during the MD trajectory can suggest a disruption of the binding interface.⁵⁵

3.6. Water at the Protein/Antibody Interface. Water plays an important role in biomolecular binding processes. Figure 10 displays the number of water molecules close to the protein's binding site in the complex and free MD trajectories. It is expected that, upon antibody binding, the protein loses some of the solvent that is in close contact with the protein's polar groups. Indeed, this is exactly what has been observed.

In the free MD trajectory, the number of water molecules that were found in proximity to the protein ranged between 15 and 40 and averaged at 27.7 (3.7). In the complex MD trajectory, this quantity ranged between 20 and 49 and averaged at 34.8 (3.8). Thus, the Pvs25 protein lost approximately seven water molecules from its first solvation shell, upon binding to the 2A8 antibody.

Another important finding of these calculations was a water-bridged hydrogen bond between Glu₅₉ protein's residue and Asp_{101H} from the antibody's CDR3 heavy chain. The Glu₅₉:O^{ε2} atom and Asp_{101H}:O^{δ1} or Asp_{101H}:O^{δ2} atom participated in this water-bridged hydrogen bond interaction from the whole trajectory. It must be noted that Asp_{101H}'s side chain also made a salt bridge with the protein's Lys₄₄ side chain.

4. Conclusions

Pvs25 is an essential protein for Plasmodium parasites to infect mosquitoes and currently is a leading candidate for a transmission-blocking malaria vaccine. Pvs25's structure is characterized by the presence of 11 disulfide bonds, a unique feature in the protein structure of approximately 180 residues. Thus, a detailed atomistic view of the dynamics of these loops can elucidate important views in order to design potential loop mimetics for a potential transmission-blocking malaria vaccine. To hit this target, we employed molecular dynamics simulations of the Pvs25 protein in free and complex forms with the 2A8 antibody.

The results presented in this study provide accumulated evidence of the role of the 51–71 loop in the recognition of

the Pvs25 protein by the 2A8 antibody. The flexibility of this loop significantly reduced upon antibody–antibody binding, as indicated by RMSF, RMSD, dDCA, and configurational entropy analysis. The reduction in configurational entropy is directly correlated by interactions made by selective residues at the protein/antibody interface. Our results are in very good agreement with similar studies in the literature and provide more evidence about the important role of biomolecular plasticity in the protein's functionality.

Interestingly, we found out that the protein's configurational entropy remained virtually the same, before and after the binding. However, entropy reduction in some loops was accompanied with an entropy increase in other parts of the protein. A detailed look at loop and per residue configurational entropy results revealed that a significant entropy reallocation occurred after antibody binding of the protein, with direct dependence on the distance from the main loop (51–71) that contacts the antibody's binding site. The corroboration of RMSF, RMSD, and dPCA results with the entropy analysis further supports these findings.

Acknowledgment. Parallel execution of NAMD was performed at the Research Center for Scientific Simulations (RCSS) of the University of Ioannina. The open source community (Linux, NAMD, GNU etc) is gratefully acknowledged for public release of all the necessary computer software needed for this research work.

Supporting Information Available: The modified PDB file 1z27, with difference of backbone entropy as the B factor column (used to produce Figure 7), is available free of charge via the Internet at <http://pubs.acs.org>.

References

- Escalante, A. A.; Cornejo, O. E.; Freeland, D. E.; Poe, A. C.; Durrego, E.; Collins, W. E.; Lal, A. A. A monkey's tale: The origin of *Plasmodium vivax* as a human malaria parasite. *Proc. Natl. Acad. Sci. U.S.A.* **2005**, *102*, 1980–1985.
- Tsuboi, T.; Kaslow, D. C.; Gozar, M. M.; Tachibana, M.; Cao, Y. M.; Torii, M. Sequence polymorphism in two novel *Plasmodium vivax* ookinete surface proteins, Pvs25 and Pvs28, that are malaria transmission-blocking vaccine candidates. *Mol. Med.* **1998**, *4*, 772–782.
- Lim, C. S.; Tazi, L.; Ayala, F. J. *Plasmodium vivax*: Recent world expansion and genetic identity to *Plasmodium simium*. *Proc. Natl. Acad. Sci. U.S.A.* **2005**, *102*, 15523–15528.
- Gunawardena, S.; Karunaweera, N. D.; Ferreira, M. U.; Phone-Kyaw, M.; Pollack, R. J.; Alifrangis, M.; Rajakaruna, R. S.; Konradsen, F.; Amerasinghe, P. H.; Schousboe, M.; Galappaththy, G. N. L.; Abeyasinghe, R. A.; Hartl, D. L.; Wirth, D. F. Geographic Structure of *Plasmodium vivax*: Microsatellite Analysis of Parasite Populations from Sri Lanka, Myanmar, and Ethiopia. *Am. J. Trop. Med. Hyg.* **2010**, *82*, 235–242.
- Tomas, A. M.; Margos, G.; Dimopoulos, G.; van Lin, L. H. M.; de Koning-Ward, T. F.; Sinha, R.; Lupetti, P.; Beetsma, A. L.; Rodriguez, M. C.; Karras, M.; Hager, A.; Mendoza, J.; Butcher, G. A.; Kafatos, F.; Janse, C. J.; Waters, A. P.; Sinden, R. E. P25 and P28 proteins of the malaria ookinete surface have multiple and partially redundant functions. *EMBO J.* **2001**, *20*, 3975–3983.

- (6) Saxena, A. K.; Wu, Y.; Garboczi, D. N. Plasmodium P25 and P28 surface proteins: potential transmission-blocking vaccines. *Eukaryotic Cell* **2007**, *6*, 1260–1265.
- (7) Ramjanee, S.; Robertson, J. S.; Franke-Fayard, B.; Sinha, R.; Waters, A. P.; Janse, C. J.; Wu, Y.; Blagborough, A. M.; Saul, A.; Sinden, R. E. The use of transgenic Plasmodium berghei expressing the Plasmodium vivax antigen P25 to determine the transmission-blocking activity of sera from malaria vaccine trials. *Vaccine* **2007**, *25*, 886–894.
- (8) Saxena, A. K.; Singh, K.; Su, H. P.; Klein, M. M.; Stowers, A. W.; Saul, A. J.; Long, C. A.; Garboczi, D. N. The essential mosquito-stage P25 and P28 proteins from Plasmodium form tile-like triangular prisms. *Nat. Struct. Mol. Biol.* **2005**, *13*, 90–91.
- (9) Gupta, A.; Van Vlijmen, H.; Singh, J. A classification of disulfide patterns and its relationship to protein structure and function. *Protein Sci.* **2004**, *13*, 2045–2058.
- (10) Aksimentiev, A.; Brunner, R.; Cohen, J.; Comer, J.; Cruz-Chu, E.; Hardy, D.; Rajan, A.; Shih, A.; Sigalov, G.; Yin, Y.; Schulten, K. Computer modeling in biotechnology: a partner in development. *Methods Mol. Biol.* **2008**, *474*, 181–234.
- (11) van Gunsteren, W. F.; Dolenc, J. Biomolecular simulation: historical picture and future perspectives. *Biochem. Soc. Trans.* **2008**, *36*, 11–15.
- (12) van Gunsteren, W. F.; Bakowies, D.; Baron, R.; Chandrasekhar, I.; Christen, M.; Daura, X.; Gee, P.; Geerke, D. P.; Glättli, A.; Hünenberger, P. H.; Kastenholz, M. A.; Oostenbrink, C.; Schenk, M.; Trzesniak, D.; van der Vegt, N. F. A.; Yu, H. B. Biomolecular modeling: Goals, problems, perspectives. *Angew. Chem., Int. Ed. Engl.* **2006**, *45*, 4064–4092.
- (13) van Gunsteren, W. F.; Dolenc, J.; Mark, A. E. Molecular simulation as an aid to experimentalists. *Curr. Opin. Struct. Biol.* **2008**, *18*, 149–53.
- (14) van der Kamp, M. W.; Schaeffer, R. D.; Jonsson, A. L.; Scouras, A. D.; Simms, A. M.; Toofanny, R. D.; Benson, N. C.; Anderson, P. C.; Merkley, E. D.; Rysavy, S.; Bromley, D.; Beck, D. A. C.; Daggett, V. Dynameomics: A Comprehensive Database of Protein Dynamics. *Structure* **2010**, *18*, 423–435.
- (15) Oomen, C. J.; Hoogerhout, P.; Bonvin, A. M. J. J.; Kuipers, B.; Brugghe, H.; Timmermans, H.; Haseley, S. R.; van Alphen, L.; Gros, P. Immunogenicity of peptide-vaccine candidates predicted by molecular dynamics simulations. *J. Mol. Biol.* **2003**, *328*, 1083–1089.
- (16) Mallik, B.; Morikis, D. Applications of Molecular Dynamics Simulations in Immunology: A Useful Computational Method in Aiding Vaccine Design. *Curr. Proteomics* **2006**, *3*, 259–270.
- (17) Galeazzi, R. Molecular Dynamics as a Tool in Rational Drug Design: Current Status and Some Major Applications. *Curr. Comput.-Aided Drug Des.* **2009**, *5*, 225–240.
- (18) Stavrakoudis, A. Conformational Flexibility in Designing Peptides for Immunology: The Molecular Dynamics Approach. *Curr. Comput.-Aided Drug Des.* **2010**, *6*, 207–222.
- (19) Tantar, A. A.; Conilleau, S.; Parent, B.; Melab, N.; Brillet, L.; Roy, S.; Talbi, E. L.; Horvath, D. Docking and Biomolecular Simulations on Computer Grids: Status and Trends. *Curr. Comput.-Aided Drug Des.* **2008**, *4*, 235–249.
- (20) Markwick, P. R. L.; Bouvignies, G.; Salmon, L.; McCammon, J. A.; Nilges, M.; Blackledge, M. Toward a Unified Representation of Protein Structural Dynamics in Solution. *J. Am. Chem. Soc.* **2009**, *131*, 16968–16975.
- (21) Rashin, A. A.; Rashin, A. H. L.; Jernigan, R. L. Diversity of function-related conformational changes in proteins: coordinate uncertainty, fragment rigidity and stability. *Biochemistry* **2010**, *49*, 5683–5704.
- (22) Klepeis, J. L.; Lindorff-Larsen, K.; Dror, R. O.; Shaw, D. E. Long-timescale molecular dynamics simulations of protein structure and function. *Curr. Opin. Struct. Biol.* **2009**, *19*, 120–127.
- (23) Berman, H. M.; Battistuz, T.; Bhat, T. N.; Bluhm, W. F.; Bourne, P. E.; Burkhardt, K.; Feng, Z.; Gilliland, G. L.; Iype, L.; Jain, S.; Fagan, P.; Marvin, J.; Padilla, D.; Ravichandran, V.; Schneider, B.; Thanki, N.; Weissig, H.; Westbrook, J. D.; Zardecki, C. The Protein Data Bank. *Acta Crystallogr., Sect. D: Biol. Crystallogr.* **2002**, *58*, 899–907.
- (24) Word, J. M.; Lovell, S. C.; Richardson, J. S.; Richardson, D. C. Asparagine and glutamine: using hydrogen atom contacts in the choice of side-chain amide orientation. *J. Mol. Biol.* **1999**, *285*, 1735–1747.
- (25) MacKerell Jr, A. D.; Feig, M.; Brooks, C. L. Improved Treatment of the Protein Backbone in Empirical Force Fields. *J. Am. Chem. Soc.* **2004**, *126*, 698–699.
- (26) MacKerell Jr, A. D.; Feig, M.; Brooks, C. L. Extending the treatment of backbone energetics in protein force fields: Limitations of gas-phase quantum mechanics in reproducing protein conformational distributions in molecular dynamics simulations. *J. Comput. Chem.* **2004**, *25*, 1400–1415.
- (27) Buck, M.; Bouquet-Bonnet, S.; Pastor, R. W.; MacKerell Jr, A. D. Importance of the CMAP correction to the CHARMM22 protein force field: dynamics of hen lysozyme. *Biophys. J.* **2006**, *90*, 36–38.
- (28) Stavrakoudis, A. Molecular dynamics simulations of an apolipoprotein derived peptide. *Chem. Phys. Lett.* **2008**, *461*, 294–299.
- (29) Humphrey, W.; Dalke, A.; Schulten, K. VMD: Visual Molecular Dynamics. *J. Mol. Graphics* **1996**, *14*, 33–38.
- (30) Darden, T.; York, D.; Pedersen, L. Particle Mesh Ewald: An $\mathcal{N} \log(N)$ method for Ewald sums in large systems. *J. Chem. Phys.* **1993**, *98*, 10089–1092.
- (31) Ryckaert, J. P.; Ciccotti, G.; Berendsen, H. J. C. Numerical integration of the Cartesian equations of motion of a system with constraints: molecular dynamics of n-alkanes. *J. Comput. Phys.* **1977**, *23*, 327–341.
- (32) Feller, S. E.; Zhang, Y.; Pastor, R. W.; Brooks, B. R. Constant pressure molecular dynamics simulation: The Langevin piston method. *J. Chem. Phys. B* **1995**, *103*, 4613–4621.
- (33) Tsoulos, I. G.; Stavrakoudis, A. Eucb: a C++ program for molecular dynamics trajectory analysis. *Comput. Phys. Commun.* **2010**, Accepted. DOI: 10.1016/j.cpc.2010.11.032.
- (34) Glykos, N. M. Carma: a molecular dynamics analysis program. *J. Comput. Chem.* **2006**, *27*, 1765–1768.
- (35) Döker, R.; Maurer, T.; Kremer, W.; Neidig, K.; Kalbitzer, H. R. Determination of mean and standard deviation of dihedral angles. *Biochem. Biophys. Res. Commun.* **1999**, *257*, 348–350.
- (36) Stavrakoudis, A. A disulfide linked model of the complement protein C 8 γ complexed with C 8 α indel peptide. *J. Mol. Model.* **2009**, *15*, 165–171.

- (37) Jolliffe, I. T. *Principal component analysis*; Springer: New York, 2002.
- (38) Mu, Y.; Nguyen, P. H.; Stock, G. Energy landscape of a small peptide revealed by dihedral angle principal component analysis. *Proteins: Struct Funct Bioinfo* **2005**, *58*, 45–52.
- (39) Maisuradze, G. G.; Leitner, D. M. Free energy landscape of a biomolecule in dihedral principal component space: Sampling convergence and correspondence between structures and minima. *Proteins: Struct Funct Bioinfo* **2007**, *67*, 569–578.
- (40) Altis, A.; Otten, M.; Nguyen, P. H.; Hegger, R.; Stock, G. Construction of the free energy landscape of biomolecules via dihedral angle principal component analysis. *J. Chem. Phys.* **2008**, *128*, 245102.
- (41) Schäfer, H.; Mark, A. E.; van Gunsteren, W. F. Absolute entropies from molecular dynamics simulation trajectories. *J. Chem. Phys.* **2000**, *113*, 7809–7817.
- (42) Grünberg, R.; Nilges, M.; Leckner, J. Flexibility and Conformational entropy in Protein-Protein Binding. *Structure* **2006**, *14*, 683–693.
- (43) Schlitter, J. Estimation of absolute and relative entropies of macromolecules using the covariance matrix. *Chem. Phys. Lett.* **1993**, *215*, 617–621.
- (44) Hsu, S.-T. D.; Peter, C.; van Gunsteren, W. F.; Bonvin, A. M. J. J. Entropy calculation of HIV-1 Env gp120, its receptor CD4, and their complex: an analysis of configurational entropy changes upon complexation. *Biophys. J.* **2005**, *88*, 15–24.
- (45) *Numerical Recipes in C: The Art of Scientific Computing*, 3rd ed.; Press, W. H., Teukolsky, S. A., Vetterling, W. T., Flannery, B. P., Eds.; Cambridge University Press: Cambridge, U. K., 1992.
- (46) Missimer, J. H.; Steinmetz, M. O.; Baron, R.; Winkler, F. K.; Kammerer, R. A.; Daura, X.; van Gunsteren, W. F. Configurational entropy elucidates the role of salt-bridge networks in protein thermostability. *Protein Sci.* **2007**, *16*, 1349–59.
- (47) Hubbard, S. Naccess V2.1.1 - Atomic Solvent Accessible Area Calculations. <http://www.bioinf.manchester.ac.uk/naccess> (accessed Dec 2010).
- (48) Maisuradze, G. G.; Liwo, A.; Scheraga, H. A. Principal component analysis for protein folding dynamics. *J. Mol. Biol.* **2009**, *385*, 312–329.
- (49) Lee, A.; Kinnear, S.; Wand, A. Redistribution and loss of side chain entropy upon formation of a calmodulin-peptide complex. *Nat. Struct. Biol.* **2000**, *7*, 72–77.
- (50) Frederick, K. K.; Marlow, M. S.; Valentine, K. G.; Wand, A. J. Conformational entropy in molecular recognition by proteins. *Nature* **2007**, *448*, 325–329.
- (51) Huang, J.; Honda, W. CED: a conformational epitope database. *BMC Immunol.* **2006**, *7*, 7.
- (52) Olsson, T. S. G.; Williams, M. A.; Pitt, W. R.; Ladbury, J. E. The thermodynamics of protein–ligand interaction and solvation: Insights for ligand design. *J. Mol. Biol.* **2008**, *384*, 1002–1007.
- (53) Rashin, A. Buried Surface Area Conformational Entropy, and Protein Stability. *Biopolymers* **1984**, *23*, 1605–1620.
- (54) Novotny, M.; Seibert, M.; Kleywegt, G. J. On the precision of calculated solvent-accessible surface areas. *Acta Crystallogr., Sect. D* **2007**, *D63*, 270–274.
- (55) Stavrakoudis, A. Computational modeling and molecular dynamics simulations of a cyclic peptide mimotope of the CD52 antigen complexed with CAMPATH-1H antibody. *Mol. Simul.* **2010**, *36*, 127–137.

CT100543C